

Entraining in trout: a behavioural and hydrodynamic analysis

Anja Przybilla^{1,*}, Sebastian Kunze², Alexander Rudert², Horst Bleckmann¹ and Christoph Brücker²

¹Institute of Zoology, University of Bonn, Poppelsdorfer Schloss, 53115 Bonn, Germany and ²Institute of Mechanics and Fluid Dynamics, TU Bergakademie Freiberg, Lampadiusstr. 4, 09599 Freiberg, Germany

*Author for correspondence (przyb@uni-bonn.de)

Accepted 26 April 2010

SUMMARY

Rheophilic fish commonly experience unsteady flows and hydrodynamic perturbations. Instead of avoiding turbulent zones though, rheophilic fish often seek out these zones for station holding. A behaviour associated with station holding in running water is called entraining. We investigated the entraining behaviour of rainbow trout swimming in the wake of a D-shaped cylinder or sideways of a semi-infinite flat plate displaying a rounded leading edge. Entraining trout moved into specific positions close to and sideways of the submerged objects, where they often maintained their position without corrective body and/or fin motions. To identify the hydrodynamic mechanism of entraining, the flow characteristics around an artificial trout placed at the position preferred by entraining trout were analysed. Numerical simulations of the 3-D unsteady flow field were performed to obtain the unsteady pressure forces. Our results suggest that entraining trout minimise their energy expenditure during station holding by tilting their body into the mean flow direction at an angle, where the resulting lift force and wake suction force cancel out the drag. Small motions of the caudal and/or pectoral fins provide an efficient way to correct the angle, such that an equilibrium is even reached in case of unsteadiness imposed by the wake of an object.

Key words: entraining, fish locomotion, hydrodynamics, swimming kinematics, rainbow trout.

INTRODUCTION

Rheophilic fish commonly experience unsteady flows and hydrodynamic perturbations associated with physical structures like rocks and branches. How rheophilic fish deal with unsteady flow conditions is of ecological and commercial importance and is the subject of many field and laboratory studies (Fausch, 1984; Fausch, 1993; Gerstner, 1998; Heggenes, 1988; Heggenes, 2002; McLaughlin and Noakes, 1998; Pavlov et al., 2000; Shuler et al., 1994; Smith and Brannon, 2005; Webb, 1998). It has recently been investigated how rainbow trout, *Oncorhynchus mykiss*, interact with unsteady flow regimes (Liao, 2004; Liao, 2006; Liao et al., 2003a; Liao et al., 2003b). At Reynolds numbers (Re) beyond 140 (see Eqn 1), flow behind a bluff 2-D body object, such as a cylinder, generates a staggered array of discrete, periodically shed, columnar vortices of alternating sign. This flow pattern is called a Kármán vortex street (Vogel, 1996). Trout exposed to a Kármán vortex street hold station by either swimming with undulating motions in the region of reduced flow behind the object (drafting) or by swimming directly in the vortex street displaying a swimming kinematic that synchronises with the shed vortices (Kármán gait) (Liao, 2004; Liao, 2006; Liao et al., 2003a; Liao et al., 2003b). For station holding, trout also use the high-pressure, reduced-flow bow wake zone in front of the object (Liao et al., 2003a). Compared with trout swimming in undisturbed, unidirectional flow, there is a reduction of locomotory costs during Kármán gaiting and swimming in the bow wake. This is evident from a reduced tail-beat frequency during these behaviours and from a decrease in red muscle activity during Kármán gaiting (Liao, 2004; Liao et al., 2003a; Liao et al., 2003b).

Another behaviour rheophilic fish may use to save locomotory costs is entraining. Entraining fish move into a stable position close to and sideways of an object, where they hold station by irregular axial swimming and/or fin motions (Liao, 2006; Liao, 2007; Sutterlin and Waddy, 1975; Webb, 1998). This suggests that fish

try to optimise their position in response to unsteadiness in the wake of the object. Another observation is that entraining fish angle their bodies away from the object and the main flow direction, which exists upstream of the object. The hydrodynamic reason for this is still unknown (Liao, 2007). Therefore, we reinvestigated the entraining behaviour of trout. In our study, entraining was the most common behaviour of trout that were confronted with a D-shaped cylinder or with a semi-infinite flat plate displaying a rounded leading edge. Based on the results of computational fluid dynamics (CFD), we propose a hydrodynamic mechanism that can explain the fish's movements during entraining.

MATERIALS AND METHODS

Behavioural experiments

Experimental animals

Thirty-six rainbow trout, *Oncorhynchus mykiss* (Walbaum 1792, total body length L 14.1±2.1 cm, mean ± s.d.), were used for the experiments. Trout were purchased from a local dealer, held individually in 45 l aerated freshwater aquaria (water temperature 13±1°C, light:dark cycle 10h:14h) and fed daily with fish pellets.

Experimental setup

Experiments were performed in a custom-made flow tank (1000 l, water temperature 13±1°C), consisting of an entrance cone (constriction ratio 3:1) and a working section (width 28 cm, height 40 cm, length 100 cm, water level 28 cm) made of transparent Perspex[®], delineated within the flow tank by upstream and downstream nets (mesh width 1 cm, fibre diameter 0.02 cm). Flow was generated by two propellers (Kaplan propellers, 23 cm×30 cm, Gröver Propeller GmbH, Köln, Germany), located downstream of the working section. These were coupled to a DC motor (SRF 10/1, Walter Flender Group, Düsseldorf, Germany). To avoid coarser-scale eddies in the working section, the water was directed through

a collimator (inner tube diameter 0.4 cm, tube length 4 cm) and two turbulence grids (mesh widths 0.5 cm and 0.25 cm, wire diameters 0.1 cm and 0.05 cm). In previous experiments trout often swam close to the bottom of the working section. To avoid this, a net (mesh width 1 cm, fibre diameter 0.02 cm) was mounted 4 cm over the bottom of the working section. Two 150 W halogen lights were installed above the working section.

A solid black polyvinyl chloride cylinder (diameter 5 cm) was lengthwise cut in half (D-shaped cylinder, hereafter referred to as 'cylinder') and placed vertically in the working section of the flow tank, approximately 30 cm downstream of the upstream net, to generate hydrodynamic perturbations (cf. Fig. 1A, Fig. 2). Trout use the water motions caused by the cylinder not only for Kármán gaiting (Liao, 2004; Liao, 2006; Liao et al., 2003a; Liao et al., 2003b) but also for entraining (Liao, 2006; Montgomery et al., 2003; Sutterlin and Waddy, 1975; Webb, 1998) and swimming in the bow wake (Liao et al., 2003a).

A Kármán vortex street will only be generated over a certain range of Reynolds numbers, typically above 140. The Reynolds number Re is a dimensionless index that gives a measure for the ratio of inertial forces to viscous forces. The Reynolds number is calculated according to the formula:

$$Re = \frac{\rho \cdot D \cdot U}{\mu}, \quad (1)$$

where ρ is the fluid density (999.38 kg m^{-3} at 13°C), D the cylinder diameter (5 cm) or fish length ($14.1 \pm 2.1 \text{ cm}$, mean \pm s.d.), U the actual flow velocity in the region of the cylinder (see Eqn 3) and μ the fluid viscosity ($1.2155 \times 10^{-3} \text{ Pas}^{-1}$, 13°C) (Vogel, 1996).

The frequency of vortex detachment is called vortex-shedding frequency (VSF). The VSF is a function of the Strouhal number St (a dimensionless index), the diameter D of the cylinder and the actual flow velocity U (Vogel, 1996):

$$VSF = \frac{St \cdot U}{D}. \quad (2)$$

The Strouhal number for the cylinder depends on the Reynolds number; however, it reaches an almost constant value of 0.2 for $Re > 2000$. The projected area of the cylinder was 17.8% of the cross-sectional area of the working section. To account for flow constrictions near the cylinder due to blocking effects, the VSF was calculated using the actual flow velocity U in the region of the cylinder, according to an ansatz typically used for vortex flow meters (Igarashi, 1999; Liao et al., 2003a):

$$U = U_\infty \cdot \frac{W}{W - D}, \quad (3)$$

where U_∞ is the nominal flow velocity (42 cm s^{-1} in our experiments) and W the width of the flow tank (28 cm). For the behavioural experiments a Reynolds number of 20,000, based on the diameter of the cylinder, was chosen.

Particle image velocimetry (PIV) was used to monitor the flow field in the working section of the flow tank and to verify the calculated VSF (cf. Eqns 2 and 3). Neutrally buoyant polyamide particles (diameter $50 \mu\text{m}$, Dantec Dynamics, Skovlunde, Denmark) were seeded in the flow tank and illuminated with a light sheet generated with a high-speed PIV laser (Newport, LaVision Inc., Göttingen, Germany). The laser sheet was oriented parallel to the water surface, approximately 10 cm above the bottom of the working section. Particles were recorded with a high-speed camera ($250 \text{ frames s}^{-1}$, FlowMaster HSS-4, LaVision Inc.; recording software: Photron Fastcam Viewer PFV, Photron USA Inc., San

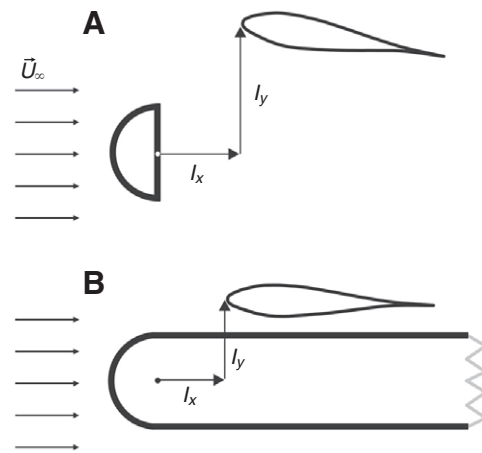


Fig. 1. Experimental setup showing the mean position of trout entraining on the right side of a D-shaped cylinder (A, cylinder diameter 5 cm) and a semi-infinite flat plate displaying a rounded leading edge (B, width 5 cm, length 35 cm). l_x and l_y : distance from snout to the point of origin of the object in x - and y -direction. Drawings are not to scale. U_∞ , nominal flow velocity.

Diego, CA, USA) and their movements analysed with the software DaVis Imaging 7.1 (LaVision Inc.). Both the measured and the calculated ($U_\infty = 42 \text{ cm s}^{-1}$, St 0.2) VSF were 2 Hz.

For a better understanding of the hydrodynamic mechanism of entraining, experiments with the D-shaped cylinder were compared with experiments with a semi-infinite flat plate displaying a rounded leading edge (width 5 cm, length 35 cm, height 40 cm), hereafter referred to as 'plate' (cf. Fig. 1B). The flow field around such a plate is more stable than the flow field around a cylinder (cf. Fig. 3) and it is of interest to compare the behaviour of trout during entraining. When the plate was positioned in the working section (Fig. 1B), trout preferred the bow wake zone (see below) or the region of reduced flow behind the plate. To prevent trout from entering these zones, the upstream and downstream nets were placed 10 cm upstream and 1 cm downstream of the plate.

Experimental procedures

Before each trial, trout were accustomed to the working section of the flow tank for at least 20 min. A mirror was mounted at 45° below the working section to film trout ventrally. Each trout was videotaped (25 frames s^{-1} , WV-BP 100/6, Panasonic, Hamburg, Germany) for about 30 min to assess its spatial preference in the working section. For kinematic analysis, sequences of the ventral view of trout swimming in undisturbed, unidirectional flow (free stream, FS) and of trout entraining close to and sideways of the submerged objects were videotaped (62 frames s^{-1} , RedLake MotionSCOPE M-1, Stuttgart, Germany).

The position of the trout was determined with the video analysis program VidAna (M. Hofmann, www.vidana.net), which recognises the fish's silhouette on the basis of intensity contrasts. According to Liao, four zones were specified in the working section of the flow tank (Liao, 2006). Entraining zones: the two zones close to and adjacent to the right and left side of the cylinder or the plate. Bow wake zone: the zone centred along the midline, adjacent to and upstream of the cylinder or the plate. Kármán gaiting and drafting zone: the zone centred along the midline downstream of the cylinder (see also Fig. 2).

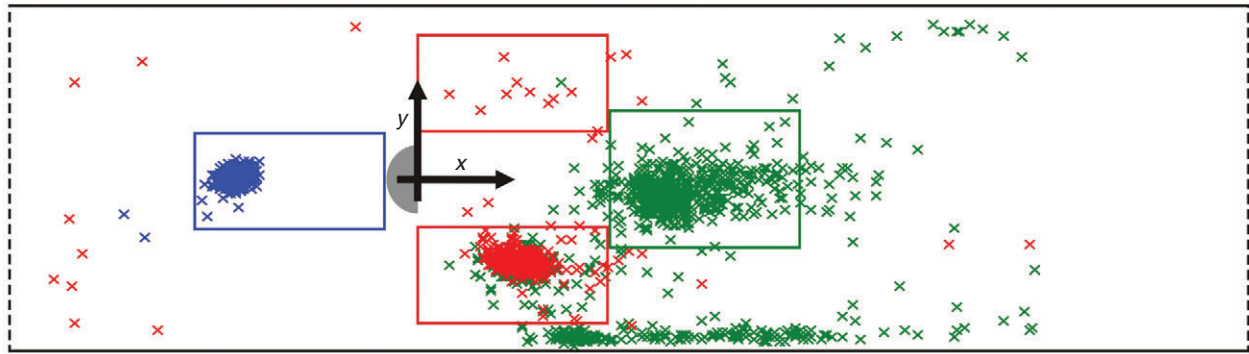


Fig. 2. Working section (width 28 cm, length 100 cm) of the flow tank in top view. Flow was from left to right. Head locations of three trout were plotted every 2 s (900 data points for each trout). Each colour represents one individual. Red rectangles: entraining zones (defined as two 7 cm×15 cm large rectangular regions on either side of the cylinder). Blue rectangle: bow wake zone (centred along the midline upstream to the cylinder, size 7 cm×15 cm). Green rectangle: Kármán gait zone (defined as a single rectangle centred along the midline of the cylinder wake, size 10 cm×15 cm). Grey half circle: D-shaped cylinder. The broken vertical lines indicate the position of the upstream and downstream net. Drawing is to scale.

To measure kinematic variables, a custom-made program (GraphicMeasurer, Ben Stöver) transferred points along the calculated body midline of the trout to a coordinate system using the centre of the cylinder's rear edge (or the corresponding point of the plate) as point of origin (cf. Fig. 1A,B). The variables tail-beat frequency, maximum lateral excursion at three body points (snout, 50% L , tail tip), mean distance from snout to the submerged object along the x - (l_x) and y -axes (l_y ; for axes see Figs 1, 2), mean body angle β relative to the x -axis (= mean direction of the undisturbed, unidirectional flow), difference between the maximum and minimum body angle within each sequence Δ , maximum difference in chord length and the displacement of the fish's body along the x - and y -axes were determined.

Kinematics were only analysed for fish swimming within the entraining zone, using sequences (high-speed camera, 62 frames s^{-1}) that lasted for at least 0.16 s (10 frames). To clearly identify no-motion sequences, i.e. sequences in which trout did not move their fins and/or body (see below), we used a time window of 0.16 s. During continuous swimming trout perform at least half a tail-beat cycle during this time. Tail-beat frequencies of entraining trout and of trout swimming in undisturbed, unidirectional flow were calculated by averaging at least five consecutive tail beats. Maximum lateral excursions of trout were calculated at three body points (snout, 50% L , tail tip) and defined as the distance between the extreme y -positions at each body point. To calculate the maximum difference in chord length, no distinction was made between U-shaped or S-shaped body profiles. Irrespective of the body profile, the distance between the snout and the tail tip was measured and expressed as a percentage of total body length L (= maximum chord length). The difference between L and the measured value was defined as the maximum difference in chord length. To calculate the displacement

of the trout with respect to the x - and y -axes, the x - and y -coordinates at 21 body points, spaced equally along the midline of the trout, were measured (see above). Mean x - and y -positions were then calculated for each frame. Displacement was defined as the distance between the most extreme means calculated for x - and y -positions within each analysed sequence. Distances to the cylinder, displacement of the trout's body along the x - and y -axes and lateral excursion at three body points are given in cylinder diameter D . In addition, it was measured how long the pectoral fins were extended during swimming. Pectoral fin extension was defined as any visible abduction of the pectoral fins from the body. We did not distinguish whether only one or both pectoral fins were extended. Sequences, in which pectoral fin movements were counted, had a duration of 66 s (62 frames s^{-1}). As the swimming behaviour of trout varied between individuals, not all trout contributed to the results with the same number of kinematic sequences.

Statistical analysis

For all kinematic variables mean values and standard deviations are determined. Selected maximum (max.) and minimum (min.) values are given in the text. Non-parametric tests were conducted because of violations of the assumption of normality and homogeneity of variance. Statistical tests were performed at an α -level of 0.05. The number of experimental animals (N) and the number of single observations (n) are given for all behavioural experiments.

Numerical model

The model applied to the numerical calculations is based on the fundamental equations of fluid mechanics, i.e. the Navier–Stokes equations, which describe the conservation of mass and momentum. Results show the distribution of all flow variables in each position for the calculated range over time. In consideration of the geometry, all calculations were made three-dimensionally. The fundamental equations are:

$$\frac{\partial \rho}{\partial t} + \frac{\partial}{\partial x_i} (\rho U_i) = 0, \quad (4)$$

$$\frac{\partial}{\partial t} (\rho U_i) + \frac{\partial}{\partial x_j} (\rho U_j U_i) = -\frac{\partial P}{\partial x_i} + \eta_t \frac{\partial^2 U_i}{\partial x_j^2} + \rho g_i. \quad (5)$$

Turbulence, represented by the turbulent viscosity η_t , is described by the k - ϵ model (Launder and Sharma, 1974). It is a two-equation

Table 1. Overview of the relevant model parameters

Parameter	Simulation	Experiment
Diameter of cylinder D (cm)	5	10
Total body length of fish L (cm)	14	28
Incoming flow velocity U_∞ (cm s^{-1})	42	21
Reynolds number Re	20,000	20,000
Strouhal number St	0.21	0.21
Body angle β (deg)	11	11
Distance along x -axis l_x (D)	0.55	0.55
Distance along y -axis l_y (D)	1.38	1.38

Table 2. Boundary conditions (OpenFOAM UserGuide)

Part	Velocity vector U (cm s ⁻¹)	Turbulent kinetic energy k (cm ² s ⁻²)	Turbulent kinetic dissipation rate ϵ (cm ² s ⁻³)	Pressure p (Pa)
Inlet	fixed value $U_x=42$	fixed value $k=174.96$	fixed value $\epsilon=2756$	zero gradient $\nabla p=0$
Outlet	zero gradient $\nabla U_x=0$ $\nabla U_y=0$ $\nabla U_z=0$	zero gradient $\nabla k=0$	zero gradient $\nabla \epsilon=0$	fixed value $p=0$
Walls	fixed value $U_x=0$ $U_y=0$ $U_z=0$	zero gradient $\nabla k=0$	zero gradient $\nabla \epsilon=0$	zero gradient $\nabla p=0$
Free surface	slip $\nabla U_x=0$ $U_y=0$ $U_z=0$	zero gradient $\nabla k=0$	zero gradient $\nabla \epsilon=0$	zero gradient $\nabla p=0$

U , actual flow velocity.

model, which includes two transport equations describing the turbulent properties of the flow. In this model, k is the turbulent kinetic energy whereas ϵ is the turbulent dissipation. ϵ determines the scale of the turbulence. The k - ϵ model gives good results for wall-bounded and internal flows. The turbulent viscosity η_t is computed from k and ϵ :

$$\eta_t = \rho C_\eta \frac{k^2}{\epsilon} \quad (6)$$

The model constant C_η is computed by the model itself. The equations for k and ϵ are:

$$\frac{\partial}{\partial t}(\rho k) + \frac{\partial}{\partial x_i}(\rho k U_i) = \frac{\partial}{\partial x_j} \left[\left(\eta + \frac{\eta_t}{\sigma_k} \right) \frac{\partial k}{\partial x_j} \right] + P_k - \rho \epsilon, \quad (7)$$

$$\begin{aligned} \frac{\partial}{\partial t}(\rho \epsilon) + \frac{\partial}{\partial x_i}(\rho \epsilon U_i) &= \frac{\partial}{\partial x_j} \left[\left(\eta + \frac{\eta_t}{\sigma_\epsilon} \right) \frac{\partial \epsilon}{\partial x_j} \right] \\ &+ C_{1\epsilon} \frac{\epsilon}{k} C_{3\epsilon} P_b - C_{2\epsilon} \rho \frac{\epsilon^2}{k}. \end{aligned} \quad (8)$$

Here, P_k is the generation of k due to the mean velocity gradients and P_b is the generation of turbulent kinetic energy due to buoyancy. $C_{1\epsilon}$, $C_{2\epsilon}$ and $C_{3\epsilon}$ are constants of the model. σ_k and σ_ϵ are the turbulent Prandtl numbers for k and ϵ , respectively (OpenFOAM User Guide) (Bardina et al., 1997; Chen and Patel, 1988; Shih et al., 1995; Versteeg and Malalasekera, 1995).

The equations of the numerical model were solved with the code OpenFOAM 1.5.1 (OpenFOAM User Guide). The result is based on the Finite volume method. The code used the UDS (upwind differencing scheme) interpolation scheme. For the discretisation of derivatives the CDS (central differencing scheme) scheme was used. The procedure employs the PISO (pressure implicit with splitting of operators) algorithm for pressure correction (Issa, 1985; Patankar, 1980).

The solution domain and its dimensions were taken from the behavioural experiments. In the computational experiments the domain consisted of an inlet, an outlet, the fish and a cylinder. A constant velocity of 42 cm s⁻¹ was set at the inlet. In the model, it is assumed that turbulent flow is fully developed when a turbulent intensity of 5% is appropriate for calculating values for k and ϵ . This is a typical value (3–10%) for fully developed turbulent channel flow. The pressure outlet was set to ambient pressure. All rigid walls fulfil the no-slip condition. The free surface was modelled as a flat

wall with zero shear stress. The values for all boundaries are given in Table 2.

An unstructured tetrahedral mesh was generated with the commercial mesh generator ICM CFD (ANSYS Inc., Canonsburg, PA, USA). In the mesh, most of the cells were concentrated in the area where the cylinder and the fish were present. Wall refinement was respected at the walls of the cylinder and the fish to resolve vortex shedding and flow structure between both objects. The number of cells was approximately 1.9 million.

The normalised pressure coefficient (C_p) is a dimensionless number, typically used for representation of pressure forces around bodies and is defined as:

$$C_p = \frac{p - p_\infty}{q}, \quad \text{with } q = \frac{\rho}{2} U_\infty^2, \quad (9)$$

where p_∞ is the pressure in the far field of the flow and q the dynamic pressure of the inflow.

Results that varied from the data obtained in the model experiment as well as all relevant parameters are given in Table 1. The position of the model is given by coordinates, normalised with the diameter of the cylinder. The model was placed at an x -distance of 0.55 D and a y -distance of 1.38 D . The model was tilted to 11 deg. According to the behavioural experiments (cf. Table 3) it was assumed that these values coincide with the critical point at which the trout just manages to hold station. Here, the influence of the cylinder displacement flow is minimal and the drag force on the trout is assumed to be at its maximum for the observed positions (see Table 1).

Physical model

To validate the numerical results, a model experiment was performed. Validation was necessary to account for the numerical error introduced by the turbulence model. An artificial fish was used to determine the velocity field around a trout while entraining. The model fish was enlarged by a ratio of 2:1, compared with the mean of the total body length L of the trout. The enlargement of the model was necessary to assure a sufficiently high optical resolution of the model and the flow field. The diameter of the cylinder was also enlarged by a factor of two, to assure the correct ratio between the length of the fish and the diameter of the cylinder. Otherwise, the experimental setup was identical to the setup used for the behavioural experiments (see Fig. 1). In the model experiments the fish was placed at the same position and body angle as the fish in the numerical calculations. A steel wire (diameter 0.3 cm) was used to

Table 3. Summary of trout kinematic variables for different experimental setups

	Cylinder experiment		Plate experiment	
	No-motion	Motion	No-motion	Motion
Distance along x-axis l_x (D)	0.92±0.31	0.99±0.48	0.77±0.05	0.78±0.11
Distance along y-axis l_y (D)	1.30±0.21	1.35±0.19	0.88±0.08	0.89±0.10
Displacement along x-axis (D)	0.07±0.04	0.07±0.03	0.05±0.03	0.05±0.02
Displacement along y-axis (D)	0.06±0.04	0.09±0.04	0.03±0.01	0.06±0.04
Lateral excursion of snout (D)	0.06±0.05	0.07±0.03	0.03±0.02	0.05±0.03
Lateral excursion of 50% L (D)	0.07±0.04	0.11±0.03	0.04±0.02	0.08±0.04
Lateral excursion of tail tip (D)	0.14±0.05	0.49±0.12	0.05±0.02	0.26±0.11
Mean body angle β relative to the x-axis (deg)	9.29±2.07	7.73±4.26	0.60±0.47	1.03±0.68
Max. – min. body angle Δ (deg)	3.30±1.28	8.03±2.84	1.70±0.95	6.98±3.00
Maximum difference in chord length (%)	0.23±0.13	2.95±1.00	0.19±0.09	1.12±0.78

All values are means \pm s.d.

hold the model at a constant position. The cylinder and the fish model were placed in a flow tank with a cross section of 40 cm×40 cm. The cylinder was slightly shifted to one side of the flow tank to maintain the correct distance between the fish model and the wall of the flow tank. The velocity of the incoming flow was pre-set at 21 cm s⁻¹, leading to a Reynolds number of 20,000, based on the diameter of the cylinder. The Strouhal number was calculated using the VSF and was in agreement in experiment and simulation, see Table 1. Standard PIV was used to determine the velocity field around the fish model. The light sheet was formed by a 120 mJ Nd:YAG laser (Solo-PIV Nd:YAG laser systems; Polytec GmbH, Waldbronn, Germany). The images were recorded *via* a surface mirror using a PCO 1600 camera (PCO AG, Kehlheim, Germany). The camera had a resolution of 1600 pixels×1200 pixels at a frequency of 8 Hz and a pulse separation of 0.002 s. To visualise the flow, VESTOSINT 2158 particles (diameter 20 μ m) were seeded into the flow. The software Dantec Dynamic Studio (Dantec Dynamics, Skovlunde, Denmark) was used to evaluate the velocity field. At first, an adaptive cross-correlation in 32 pixels×32 pixels sub windows and an overlap of 75% were used to evaluate the velocity vectors. In a second step, a peak validation algorithm was used to validate the correlation peaks. Thereafter, the velocity vectors were locally smoothed *via* a moving average filter over a 5×5 kernel. Finally, the results were averaged over the whole measurement period, i.e. 150 image pairs.

RESULTS

Behavioural experiments

Cylinder experiment

As a reference for the new experimental setup we first repeated some of the experiments performed by Liao (Liao et al., 2003a), using the cylinder. The trout ($N=30$, total observation time 890 min) swam in the entraining, bow wake and Kármán gait or drafting zone (cf. Fig. 2). Trout showed a significant difference in their preference for these three zones in the vicinity of the cylinder (Kruskal–Wallis test, $P=0.018$). The entraining zone was preferred (27.7±31.0% of the observation time) over the Kármán gait zone (7.9±17.2%; Mann–Whitney U -test, $P=0.003$). Trout spent 13.6±22.6% of the observation time entraining on the right and 14.2±25.0% entraining on the left side of the cylinder, neither preferring either side of the cylinder (Mann–Whitney U -test, $P=0.739$). Trout spent 28.3±36.3% of the time in the bow wake zone. Trout spent significantly more time in these three zones (cumulated size 465 cm², total size of the working section 2800 cm²; cf. Fig. 2), than expected by random distribution (expected percentage 16.65; Mann–Whitney U -test, $P<0.001$). In undisturbed flow, trout ($N=13$, observation time

383 min) preferred to swim close to the walls of the working section and spent only 9.3±13.3% of the time in the fictitious entraining, bow wake and Kármán gait zone (Mann–Whitney U -test, $P<0.001$). This was less than expected by random distribution (Mann–Whitney U -test, $P=0.001$).

Kinematical analysis

As expected (Liao, 2006), entraining trout positioned their head (body) downstream of and close to the sides of the cylinder without touching it (for mean entraining position see Fig. 1A). During entraining, sequences where trout had a stretched-straight body posture with the pectoral fins not extended and the body and tail fin showing no motions (no-motion sequences) interchanged with sequences of irregular body and/or pectoral and tail fin motions (motion sequences). No-motion sequences were used for kinematical analysis only, if they lasted for more than 0.16 s. The maximum duration of the no-motion sequences was 0.37 s. Motion sequences of equal length were analysed to allow for a direct comparison of the two types of entraining behaviour (no-motion vs motion behaviour). Trout ($N=6$, $n=39$) positioned themselves $0.96\pm 0.4D$

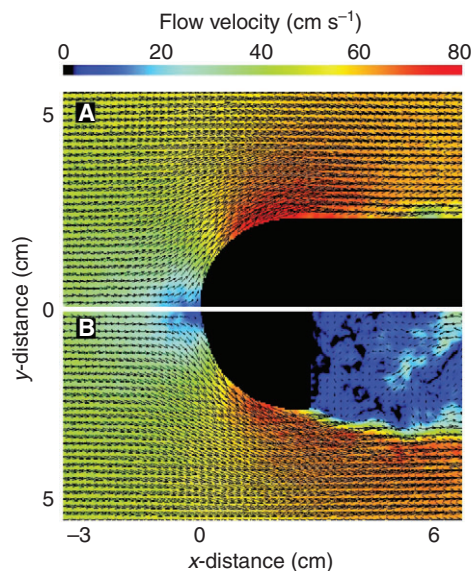


Fig. 3. Flow around a plate (A) and a cylinder (B). The flow velocity (in cm s⁻¹) is colour-coded (see colour bar on top). The vectors indicate the flow direction as well as the flow velocity (vector length). The size of each picture detail (A,B) is 5 cm×9 cm. Note that the flow around the plate is more uniform than the flow in the wake of the cylinder.

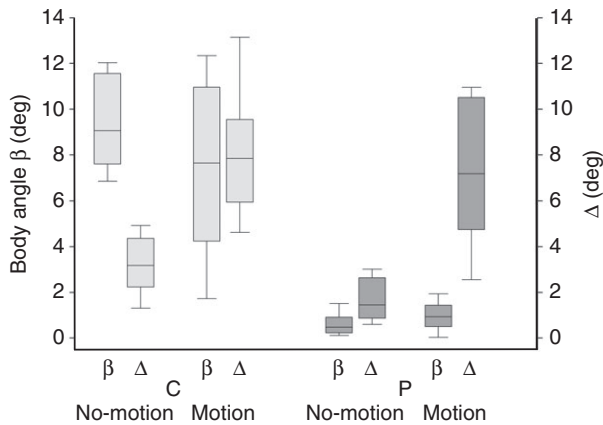


Fig. 4. Mean body angles β and the differences between maximum and minimum body angle within each sequence Δ of trout entraining in the cylinder (C) or plate experiment (P). The data are plotted as medians and interquartile ranges; whiskers are 5th and 95th percentiles.

(min. $0.27D$, max. $2.15D$) downstream and $1.33 \pm 0.2D$ (min. $0.93D$, max. $1.63D$) sideways of the cylinder (Mann–Whitney U -test, $P_{\text{distance along } x\text{-axis}}=0.955$, $P_{\text{distance along } y\text{-axis}}=0.465$; Fig. 1A and Table 3). During no-motion sequences ($N=6$, $n=19$), the maximum difference in chord length was $0.23 \pm 0.13\%$ (min. 0.1% , max. 0.6%). During the motion sequences ($N=6$, $n=20$), the maximum difference in chord length reached significantly higher values of $2.95 \pm 1.0\%$ (min. 1.5% , max. 4.9% ; Mann–Whitney U -test, $P < 0.001$; Table 3). No-motion sequences terminated after a displacement of $0.07 \pm 0.04D$ (min. $0.03D$, max. $0.14D$; x -axis) and/or $0.06 \pm 0.04D$ (min. $0.02D$, max. $0.17D$; y -axis) was reached (Table 3). Displacement along the x -axis did not differ between no-motion ($N=6$, $n=19$) and motion sequences ($N=6$, $n=20$) but differed along the y -axis (Mann–Whitney U -test, $P_{x\text{-axis}}=0.555$, $P_{y\text{-axis}}=0.046$; Table 3).

Entraining trout kept their body angled into the wake downstream of the cylinder with respect to the x -axis (Fig. 1A, Fig. 4 and Table 3). The mean body angle β did not differ between no-motion and motion sequences (Mann–Whitney U -test, $P=0.177$; Fig. 4, Table 3).

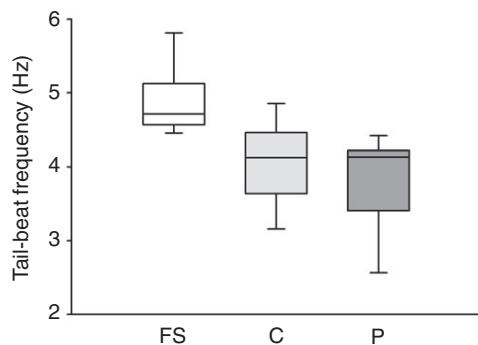


Fig. 5. Tail-beat frequencies of trout swimming in undisturbed flow (free stream, FS, flow velocity 42 cm s^{-1}) and of trout entraining close to the cylinder (C) or plate (P). Tail-beat frequencies were only measured in sequences where trout showed continuous swimming motions. The data are plotted as medians and interquartile ranges; whiskers are 5th and 95th percentiles.

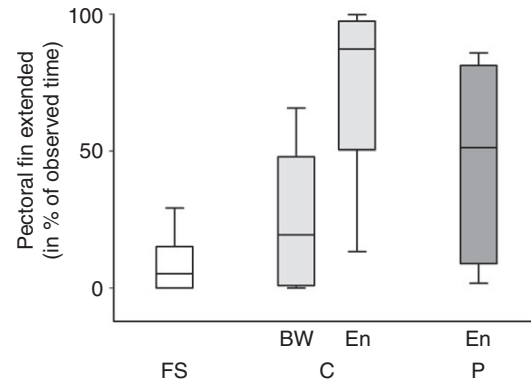


Fig. 6. Amount of time trout extended their pectoral fins. Left: free stream (FS); middle: bow wake (BW) in front of the cylinder (C) or entraining (En) in the vicinity of the cylinder; right: trout entraining next to the plate (P). All analysed sequences were recorded with a high-speed camera (62 frames s^{-1}) and lasted for 66 s. We did not distinguish between trout extending their pectoral fins on the right, left or on both body sides. The data are plotted as medians and interquartile ranges; whiskers are 5th and 95th percentiles.

However, the variation of body angle Δ was significantly larger in the motion sequences (the difference between maximum and minimum body angle within each sequence, Δ , varied between 14.16 deg and 3.36 deg) than in the no-motion sequences (5.0 deg and 1.15 deg , respectively; Mann–Whitney U -test, $P < 0.001$; Fig. 4 and Table 3). In entraining trout, the distances between the most extreme y -positions at three body points (snout, $50\% L$, tail tip) increased from anterior to posterior. For $50\% L$ and the tail tip, differences were significant between no-motion and motion sequences (Mann–Whitney U -test, $P \leq 0.003$; Table 3).

The tail-beat frequencies of entraining trout were measured only for motion sequences ($N=6$, $n=20$). In the cylinder experiment the average tail-beat frequency was $4.07 \pm 0.58 \text{ Hz}$ (min. 2.81 Hz , max. 5.08 Hz). This was significantly less than the tail-beat frequency of trout swimming in undisturbed flow ($4.9 \pm 0.46 \text{ Hz}$, min. 4.4 Hz , max. 5.89 Hz ; $N=6$, $n=19$; Mann–Whitney U -test, $P < 0.001$; Fig. 5).

Swimming trout sometimes extended their pectoral fins. During entraining (including no-motion and motion sequences), the pectoral fins were more often extended ($72.9 \pm 30.9\%$ of the observation time of 858 s; $N=8$, $n=13$; Fig. 6) than during swimming in the bow wake zone ($25.8 \pm 25.2\%$ of the observation time of 990 s; $N=7$, $n=15$; Mann–Whitney U -test, $P < 0.001$) or in undisturbed flow ($8.6 \pm 10.4\%$ of the observation time of 462 s; $N=5$, $n=7$; Mann–Whitney U -test, $P=0.001$).

Plate experiment

Trout ($N=6$) spent most ($70.8 \pm 26.9\%$) of the observation time (177 min) entraining close to the sides of the plate. With respect to the flow direction, trout were released on the left side of the working section. Trout therefore preferred entraining on the left side of the plate ($69.7 \pm 29.4\%$; right side: $1.1 \pm 2.6\%$; Mann–Whitney U -test, $P=0.004$).

Kinematical analysis

Entraining trout positioned their head (body) sideways of the plate without touching it (for mean entraining position see Fig. 1B). Trout ($N=5$, $n=47$) positioned themselves $0.78 \pm 0.08D$ (min. $0.59D$, max. $1.09D$) downstream and $0.88 \pm 0.09D$ (min. $0.72D$,

max. $1.04D$) sideways of the point of origin (Mann–Whitney U -test, $P_{\text{distance along } x\text{-axis}}=0.983$, $P_{\text{distance along } y\text{-axis}}=0.478$; Fig. 1B and Table 3). In both the no-motion and motion sequences, significant differences were observed in the trout's y -position when comparing experiments with the plate ($N=5$, $n=47$) and the cylinder ($N=6$, $n=39$; Mann–Whitney U -test, $P<0.001$). In the plate experiment, trout ($N=5$, $n=47$) swam almost parallel to the plate (Fig. 1B, Fig. 4 and Table 3). The difference between the mean body angle β in the cylinder and the plate experiment was significant (Mann–Whitney U -test, $P<0.001$; Fig. 4, Table 3). Additionally, in the plate experiment, mean body angles β were significantly smaller in the no-motion sequences ($N=5$, $n=27$) than in the motion sequences ($N=5$, $n=20$; Mann–Whitney U -test, $P=0.039$). As in the cylinder experiment (see above), the variation of body angle Δ was significantly larger in the motion (the difference between maximum and minimum body angle within each sequence, Δ , varied between 11.6 deg and 2.46 deg) than in the no-motion sequences (3.67 deg and 0.1 deg, respectively; Mann–Whitney U -test, $P<0.001$; Fig. 4, Table 3). The variation of body angle Δ was significantly larger during no-motion sequences in the cylinder experiment than in the plate experiment (Mann–Whitney U -test, $P<0.001$; Fig. 4, Table 3).

Maximum duration of the no-motion sequences was 0.81 s. No-motion sequences lasted significantly longer in the plate experiment (0.36 ± 0.14 s; $N=5$, $n=27$) than in the cylinder experiment (0.22 ± 0.07 s; $N=6$, $n=19$; Mann–Whitney U -test, $P<0.001$) but terminated after a displacement of $0.05\pm 0.03D$ (min. $0.01D$, max. $0.14D$; x -axis) and/or $0.03\pm 0.01D$ (min. $0.01D$, max. $0.06D$; y -axis) was reached (cf. Table 3). As in the cylinder experiment (see above), displacement along the y -axis was larger during motion sequences ($N=5$, $n=20$) than during no-motion sequences ($N=5$, $n=27$; Mann–Whitney U -test, $P_{x\text{-axis}}=0.966$, $P_{y\text{-axis}}=0.001$; Table 3). For both, no-motion and motion sequences, displacement was larger in the cylinder experiment (see above) than in the plate experiment ($N=11$, $n=86$; Mann–Whitney U -test, $P\leq 0.016$; Table 3).

The maximum difference in chord length during no-motion sequences ($N=5$, $n=27$) in the plate experiment was $0.19\pm 0.09\%$ (min. 0.01%, max. 0.4%). During the motion sequences, the maximum difference in chord length reached significantly higher values of $1.12\pm 0.78\%$ (min. 0.1%, max. 2.8%; $N=5$, $n=20$; Mann–Whitney U -test, $P<0.001$; Table 3). Maximum difference in chord length during the no-motion sequences in the experiment with the plate did not differ from the maximum difference in chord length during the no-motion sequences in the experiment with the cylinder (Mann–Whitney U -test, $P=0.569$; Table 3). But maximum difference in chord length during the motion sequences was significantly larger in the cylinder experiment than in the plate experiment (Mann–Whitney U -test, $P<0.001$; Table 3).

As in the cylinder experiment (see above), the differences between the most extreme y -positions at three body points (snout, 50% L , tail tip) increased from anterior to posterior. Differences in the lateral excursion at the snout, 50% L and the tail tip were significant between no-motion and motion sequences (Mann–Whitney U -test, $P\leq 0.019$; Table 3). In the plate experiment, the lateral excursion at three body points were smaller in the motion and the no-motion sequences ($N=5$, $n=47$), than in the cylinder experiment ($N=6$, $n=39$; Mann–Whitney U -test, $P\leq 0.051$).

In the plate experiment, the average tail-beat frequency of entraining trout was 3.87 ± 0.59 Hz (min. 2.56 Hz, max. 4.66 Hz; $N=5$, $n=18$). This was significantly less than the tail-beat frequency of trout swimming in undisturbed flow (4.9 ± 0.46 Hz, min. 4.4 Hz, max.

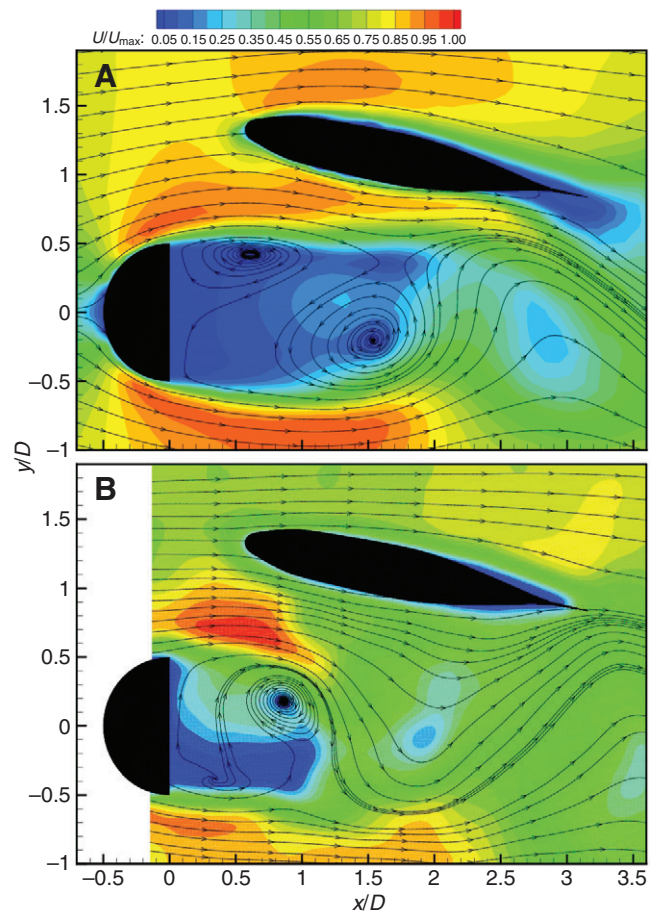


Fig. 7. Sectional streamline patterns and contours of constant normalised velocity vector U/U_{max} in the sagittal mid-plane of the fish, representing an entraining trout in the near-wake of the cylinder. The flow field depicts a certain moment in the shedding cycle, representing the unsteady and asymmetric flow character. (A) Results from the numerical simulation; (B) experimental results for a similar flow state.

5.89 Hz; $N=6$, $n=19$; Mann–Whitney U -test, $P<0.001$; Fig. 5). Tail-beat frequencies of entraining trout did not differ between experimental setups (Mann–Whitney U -test, $P=0.334$; Fig. 5).

In the plate experiment, trout ($N=5$, $n=15$) extended their pectoral fins in $43.4\pm 34.3\%$ of the observation time (990 s). This was significantly less than in the cylinder experiments (Mann–Whitney U -test, $P=0.009$; Fig. 6). However, entraining trout extended their pectoral fins more often than trout swimming in undisturbed flow (Mann–Whitney U -test, $P=0.031$) or in the bow wake in front of the cylinder (Mann–Whitney U -test, $P=0.081$; Fig. 6).

Model experiments and numerical calculations

The behavioural experiments indicated that entraining trout can hold their position at one side of a flow disturbing stationary object for distinct periods of time, with little or no body or fin movement. At this position, the flow-induced forces on the body on average cancel to zero. The flow-induced forces are specified by the wall friction and pressure distribution around the trout. To confirm this, a model trout was placed at the position preferred by real trout during entraining (cf. Table 1). To determine the characteristics of the cylinder wake flow in the presence of an entraining trout, the flow field was calculated by CFD (see Materials and methods). In addition, the velocity and pressure distribution across the surface

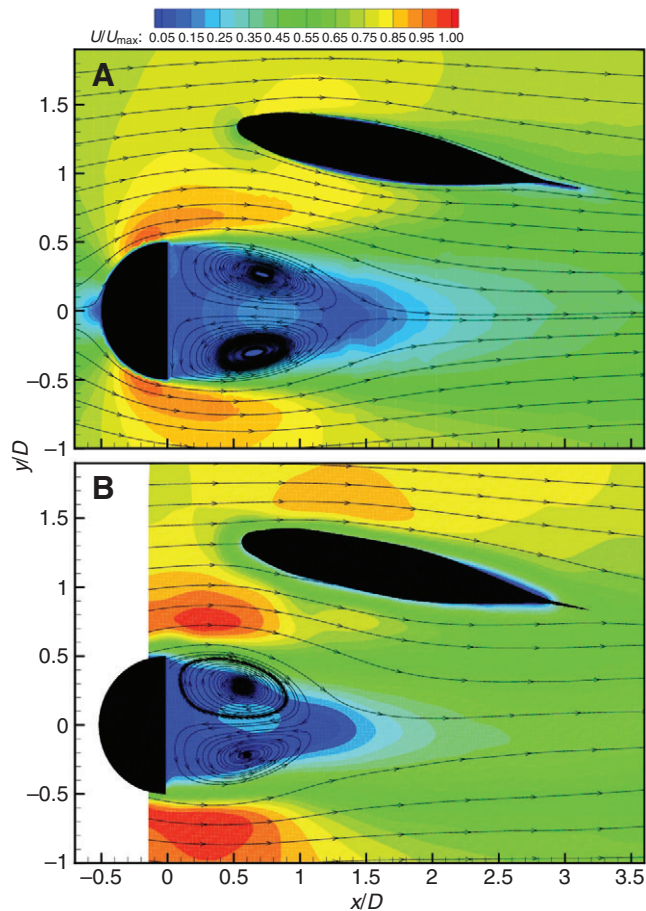


Fig. 8. Sectional streamline pattern and contours of constant normalised velocity vector U/U_{\max} in the sagittal plane of the fish, representing an entraining trout in the near-wake of a cylinder. The flow field is averaged over 35 vortex shedding cycles, representing the mean average flow around the fish while entraining. (A) Results from the numerical simulation. (B) Experimental results.

of the trout and hence the forces acting on the trout were calculated. Being in the order of micro-Newtons, these forces were difficult to measure. Fig. 7 illustrates the normalised magnitude of the velocity and the sectional streamline pattern for a momentaneous record of unsteady flow. Fig. 7A and B compare the numerical results with the model experiment for a similar flow state. The position of the cylinder and the trout model are indicated in black. The von Kármán type periodical vortex shedding can be identified in both images and is in agreement with the numerical calculations. The Strouhal number was approximated to be 0.21 in both the experiment and the numerical investigation, which is close to the Strouhal number for a cylinder of 0.2, given by Vogel (Vogel, 1996).

In the following, the focus is on the time-averaged flow field. Typically, the time-averaged velocity field contains most of the flow energy while the vortex shedding contributes to less than 20%. Fig. 8 illustrates sectional streamlines and the magnitude of the velocity of the time averaged flow field (simulation Fig. 8A and measurement Fig. 8B) in the sagittal plane of the model. One can identify the wake region downstream of the cylinder in the form of an attached separation bubble with recirculating flow. Again, simulation and experiment are in agreement. Due to the disturbance of the streamlines by the cylinder, the fish experienced a flow at its head

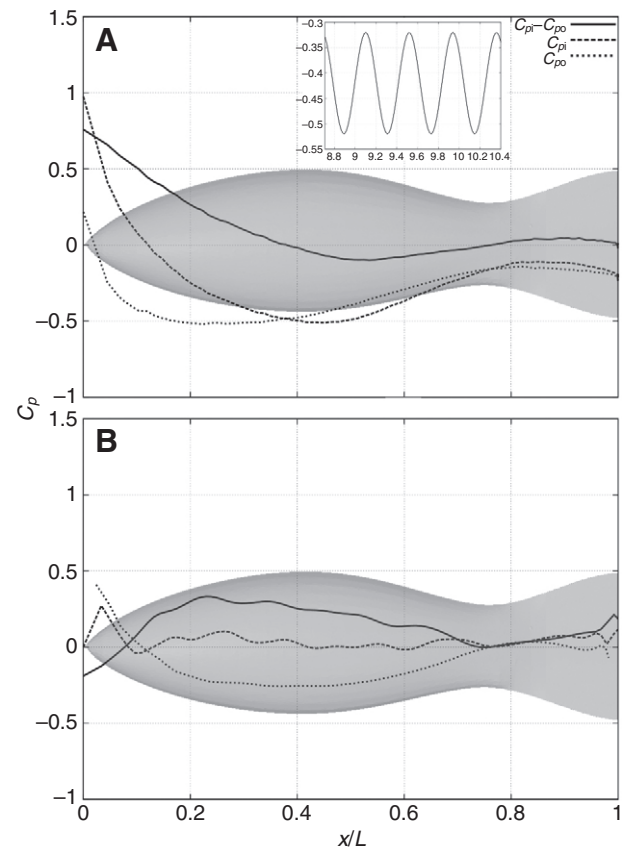


Fig. 9. Time and surface averaged distribution of $C_p = C_{pi} - C_{po}$ over the dimensionless length x/L on the fish's inside (C_{pi}) and outside (C_{po}). Values were calculated for a fish exposed to cylinder wake flow (A) and for a fish swimming in undisturbed flow (B). (A) shows the regular temporal fluctuation at $x/L = 0.5$ in the additional figure.

that was already directed upwards. Therefore, the effective body angle (denoted as the angle of attack in the airfoil theory) is the sum of the geometric angle of the body and the angle of the mean flow direction near the front of the fish. The differences in wake flow between the experimental and the numerical models, especially regarding the length of the time averaged separation bubble, resulted from shortcomings of the realisable $k-\epsilon$ turbulence models, predicting the correct contours of the separation region. The turbulent kinetic energy k was overestimated by the computational model. This leads to an elongated separation bubble.

To evaluate the full, 3-D pressure distribution on the model, the numerical results were investigated in detail. Fig. 9 shows the time averaged C_p values as discrete points on the surface of the trout over the dimensionless length x/L for both the inside (side facing the cylinder) and the outside surface of the fish. The 3-D structure of the fish is evident in the scattered distribution of the C_p values. Fig. 9A shows the values for both sides of the fish, averaged for each surface and plotted over the dimensionless length x/L . The course of this line indicates a large region of relatively small pressure differences at the mid-body region of the entraining fish ($0.4 < x/L < 1$). The described configuration is compared with a fish swimming in undisturbed, unidirectional incoming flow. The body angle was assumed to be 11 deg, the typical body angle of entraining trout in our experiments (Fig. 9B)

The results for the undisturbed flow are plotted in Fig. 9 as a solid black line. The course of C_{po} in Fig. 9B is comparable with the C_{po}

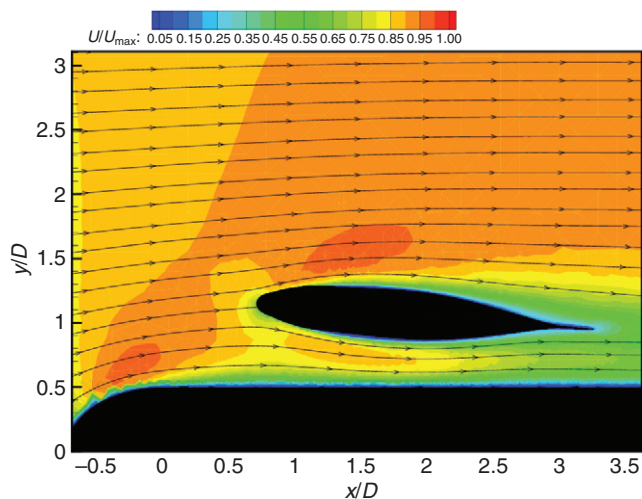


Fig. 10. Sectional streamline pattern and contours of constant normalised velocity vector U/U_{\max} in the sagittal mid-plane of the fish representing an entraining trout in the near-wake of the plate. The flow field does not show any flow separation or unsteady vortex shedding. Results are from the numerical simulation.

course in Fig. 9A. The obvious shift between both pressure profiles is caused by the effect of the cylinder on the flow around the fish. The major difference between the two configurations is evident in the course of C_{pi} . For undisturbed flow (Fig. 9B), the course of C_{pi} is shifted upwards to a higher pressure for most of the length of the trout ($0.1 < x/L < 0.8$). This results in a considerable difference between C_{pi} and C_{po} . As a measure of total force we took the average of the difference $C_p = C_{pi} - C_{po}$ over the dimensionless length of the model x/L . The resulting value for the configuration involving the cylinder is 0.06, for the configuration without any object in the undisturbed flow it is 0.16. This indicates that the influence of the cylinder on the flow, around the entraining trout, reduces the total force. As a result of the unsteady cylinder wake flow, the resulting pressure forces on the trout oscillate between a minimum value of $C_{p,\min} = -0.7$ and a maximum value of $C_{p,\max} = 1.02$. The frequency corresponds to the *VSF* in the wake of the cylinder of $f_{CP} = 1.8$ Hz. Further fine-tuning of the balance between the outer and the inner pressure field, either by moving closer to the object or by changing the body angle, may even enable the trout to cancel out the differences to zero, resulting in a perfect station holding position. Such a large number of numerical simulations, needed for the fine-tuning of the position and angle, could not be realised up to now due to the large computational effort.

Simulation of the plate experiment

Fig. 10 shows the streamlines around a plate, with the fish's body in the entraining position. The fish was angled away from the undisturbed inflow with 1 deg, which was the value obtained in the behavioural experiments. Interestingly, similar to the flow around the cylinder, the fish experienced a flow that was directed upwards, due to the flow deflection around the front part of the plate. Therefore, the effective angle of attack relative to the flow is the sum of the body angle (relative to the main flow upstream of the object) and the angle of the flow direction near the front of the fish, which was about 5 deg in the simulations. In contrast to the cylinder flow, there is no vortex shedding and thus the fish – at least in theory – has no need for corrective body and fin motions once it has reached

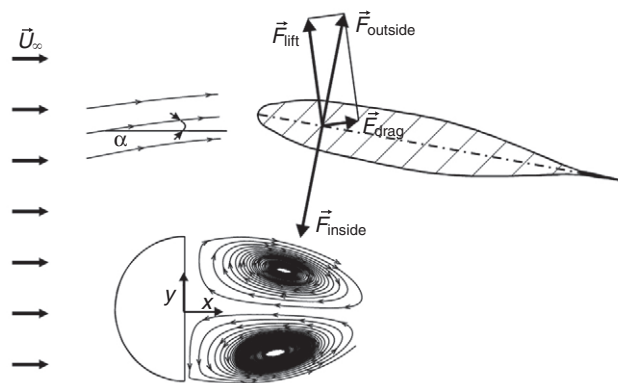


Fig. 11. Simplified sketch of the principal forces acting on an entraining fish. The virtual components of the lift and drag forces are added in the same way they would act on a 2-D airfoil without the presence of the cylinder wake and for an inflow angled to the main flow direction. F_{inside} , force on the inside of the model; F_{outside} , force on the outside of the model; F_{drag} , drag force; F_{lift} , lift force.

a stable position for entrainment. This is in agreement with the observation that trout entraining in the vicinity of the plate show less fin and body movements than trout entraining in the vicinity of the cylinder (see above).

DISCUSSION

Entraining, Kármán gaiting, drafting and swimming in the bow wake represent energetically favourable strategies for station holding in running water (for a review see Liao, 2007). As expected, the trout used in our experiments also showed these behaviours during exposure to the flow perturbations caused by a stationary cylinder. The total body length of the trout was 14.1 ± 2.1 cm, the cylinder that generated the Kármán vortex street had a diameter of 5 cm (cylinder diameter to fish length ratio was about 1:3) and the bulk flow velocity was 42 cm s^{-1} . Accordingly, the hydrodynamic requirements for Kármán gaiting were fulfilled in our experiment. Nevertheless, trout swam only $7.9 \pm 17.2\%$ of the observation time in the Kármán gait zone whereas the trout investigated by Liao (Liao, 2006) Kármán gaited in about 80% of the time. The reason for this discrepancy is unknown, but Liao et al. (Liao et al., 2003a) and Liao (Liao, 2006) already pointed out that the swimming behaviour of trout can be highly individual-specific (see also Swanson et al., 1998) and – for a given individual – may even change from day to day. Station holding strategies may also differ across species (Liao et al., 2003b). Other factors, like food availability, also influence the preferred mode for station holding (see also Fausch, 1984) (B. Baier, unpublished).

If exposed to flow perturbations caused by a cylinder, the trout preferred entraining. A cylinder exposed to bulk water flow sheds vortices in a regular pattern; therefore, the instantaneous forces that act on entraining trout fluctuate. Nevertheless, for up to 0.4 s (cylinder) and 0.8 s (plate) trout were able to hold station without any axial body and fin motions (no-motion sequences). During no-motion sequences the pectoral fins rested against the body that had a stretched-straight profile. Furthermore, the no-motion sequences were characterised by only small variations in body angle Δ (Fig. 4, Table 3). Maximum lateral body excursions were small, suggesting that for short periods of time there was no need for corrective body and/or fin motions (Table 3). The no-motion sequences alternated with sequences where trout showed irregular axial body and/or fin

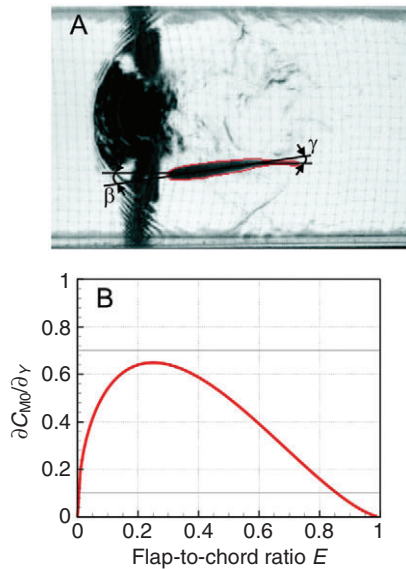


Fig. 12. (A) Image of an entraining trout adjusting its caudal fin to balance the forces and pitching moment. The body is tilted by the angle β to the main flow direction upstream of the cylinder (named herein the body angle) while the angle γ describes the tail fin angle against the body. The fish silhouette is highlighted in red. (B) Change of zero flap moment coefficient C_{M0} over the flap deflection angle for a plain flap airfoil at different flap-to-chord ratios [equation given by Glauert (Glauert, 1927)].

motions (motion sequences). During motion sequences trout showed higher lateral body excursions and a larger difference in chord length. All this suggests that entraining trout repeatedly had to balance thrust and drag forces to hold station. Obviously, without corrective body or fin motions, entraining trout were unable to maintain their position for long periods of time, most likely due to the unsteadiness of the flow behind the cylinder.

In the plate experiment trout also showed entraining behaviour. The flow field around a semi-infinite flat plate displaying a rounded leading edge is more stable than the flow field around a D-shaped cylinder (cf. Fig. 3). This is probably the reason why the no-motion sequences in the plate experiment were significantly longer than in the cylinder experiment. A significantly reduced maximum difference in chord length, pectoral fin activity as well as a reduced tail-beat frequency during the motion sequences also indicate that entraining sideways of the plate required less corrective motions than entraining downstream and sideways of the cylinder (Table 3). In general, in the plate experiment less corrective motions were seen, which can be attributed to more stable flow conditions.

The highly reduced body and fin motions during the no-motion behaviour suggest (see also Liao et al., 2003a) that station holding in the vicinity of a cylinder or a plate is energetically favourable. This agrees with a reduced muscle activity observed during entraining (A. Klein and H.B., unpublished).

Model experiments and simulations

Our model experiments suggest that entraining reduces locomotory costs. Fig. 11 illustrates the resulting forces affecting a model trout while entraining, assuming a stretched-straight body posture as observed in the behavioural experiments and a body angle similar to the body angle measured in real trout. The force components were separated in analogy to the flow around an airfoil (see Liao et al., 2003a) tilted to the flow (which is usually referred to as the

angle of attack) in a drag and lift force. An additional suction force F_{inside} acts on the model on the inner side which is due to the increased velocities in the gap between fish and cylinder wake. This simplified model was used here to demonstrate the principal effects of the body angle on the pressure distribution and the resulting forces. Because of the flow deflection near the front part of the body, entraining fish experience an upward directed flow at the nose (if the fish is entraining on the upper side of the body) and therefore, the direction of the average flow with velocity U (see Fig. 11) is already angled against the undisturbed flow U_{∞} direction far upstream of the object. According to the airfoil theory, the drag force F_{drag} is pointing in the mean flow direction of the flow U upstream of the leading edge, while the lift force F_{lift} is perpendicular to it. This results in a force F_{outside} , similar to drawing the forces for a symmetrical profile at an angle of attack. In phases of no-motion during entraining, the fish seem to keep a stable position downstream and sideways of the cylinder because the lift force F_{outside} is balanced by the counter-acting suction force F_{inside} . Thus, at a specific position next to the cylinder, and for a specific body angle, it is possible that these forces sum up to zero and fish therefore can maintain their position without any active body or fin movements. A similar hydrodynamic argument based on the aerodynamic theory has been used to describe the force balance of dolphin while riding on free surface bow waves (Hayes, 1953).

The behavioural observations have shown that trout keep their station holding position by adjusting their body angle relative to the main flow. Corrective motions for fine-tuning of the body angle result either from movements of the pectoral fins (see also Liao, 2006; Webb, 1998) and/or the caudal fin. The pectoral fins seem to play a specifically important role, because they were unusually often spread without any obvious pattern of activity during entraining (Fig. 6). Although, adjusting their body angle away from the flow by turning their caudal fin (effectively adjusting the angle of attack) may be of similar importance, as it was observed in most corrective actions. This may reflect a highly optimised adaptation in fish, as proposed by Brücker (Brücker, 2006) based on an aerodynamic theory. As a highly simplified model of the oblate fish body, he compared body and fin with an airfoil (the body) with a hinged flap (the fin). In this model, the flap length represents the caudal fin, measured from the peduncle to the trailing edge of the fin, and the chord length represents the total fish length L . In the airfoil model the zero moment coefficient, which is the rate of change of pitching moment of the foil at constant lift, is given by:

$$\frac{\partial C_{M0}}{\partial \gamma} = -2\sqrt{E - (1 - E)^3}, \quad (10)$$

according to the solution of Glauert (Glauert, 1927), with E being the flap-to-chord ratio and γ being the flap deflection angle (cf. Fig. 12A). The results of Glauert demonstrated that $\partial C_{M0}/\partial \gamma$ is maximum at approximately $E=0.2$ (cf. Fig. 12B). In other words, the rate of change of pitching moment and therefore the change of body angle against the flow (swimming direction) are highest for $E=0.2$ for any slight change in γ (caudal fin angle). Surprisingly, trout actually have a ratio of fin-to-body length of roughly $E=0.2$. Consequently, the highly simplified airfoil model gives an idea of the mechanisms trout may employ to correct their station holding position in a fast and efficient manner. Accordingly, during entraining at an optimum position, it is hypothesised that trout are able to correct body angle changes by performing only small caudal fin movements. Such corrective motions of the caudal fin were indeed observed during the present study. Future work will therefore focus on providing evidence for the hypothesis provided by the numerical flow simulations

assessing a fish model at different caudal fin angles relative to the body.

LIST OF ABBREVIATIONS

BW	bow wake
C	D-shaped cylinder
C_p	normalised pressure coefficient
C_{pi}	pressure on the inside of the model
C_{po}	pressure on the outside of the model
$C_{p,max.}$	maximum pressure coefficient
$C_{p,min.}$	minimum pressure coefficient
C_η	model constant
$C_{1\epsilon}, C_{2\epsilon}, C_{3\epsilon}$	model constants
CDS	central differencing scheme
CFD	computational fluid dynamics
D	cylinder diameter
E	flap-to-chord ratio
En	entraining
F_{drag}	drag force
F_{inside}	force on the inside of the model
F_{lift}	lift force
$F_{outside}$	force on the outside of the model
FS	free stream
k	turbulent kinetic energy
L	total body length of fish
l_x	distance from snout to submerged object along x -axis
l_y	distance from snout to submerged object along y -axis
n	number of observations
N	number of experimental animals
P	semi-infinite plate displaying a rounded leading edge
P_b	generation of turbulent kinetic energy due to buoyancy
p_∞	pressure in the far field of the flow
PISO	pressure implicit with splitting of operators
PIV	particle image velocimetry
P_k	generation of k due to the mean velocity gradients
q	dynamic pressure of the inflow
Re	Reynolds number
St	Strouhal number
U	actual flow velocity
U_∞	nominal flow velocity
UDS	upwind differencing scheme
V_{SF}	vortex-shedding frequency
W	width of flow tank
β	mean body angle
Δ	difference between maximum and minimum body angle
ϵ	turbulent dissipation
η_t	turbulent viscosity
μ	fluid viscosity
ρ	fluid dynamics
σ_k	turbulent Prandtl numbers for k
σ_ϵ	turbulent Prandtl numbers for ϵ

ACKNOWLEDGEMENTS

We thank R. Zelick and V. Schlüssel for critically reading an early draft of the manuscript. A. Klein deserves thanks for his help with the PIV studies. This work was supported by the DFG (BL 242/12 and BR 1494/10).

REFERENCES

- Bardina, J. E., Huang, P. G. and Coakley, T. J. (1997). Turbulence modeling validation, testing and development. *NASA Technical Memorandum 110446*.
- Brücker, C. (2006). *Dynamic Interaction in Bluff Body Wakes*. Habilitation, RWTH Aachen: Shaker Verlag.
- Chen, H. C. and Patel, V. C. (1988). Near-wall turbulence models for complex flows including separation. *AIAA J.* **26**, 641-648.
- Fausch, K. D. (1984). Profitable stream positions for salmonids: relating specific growth rate to net energy gain. *Can. J. Zool.* **62**, 441-451.
- Fausch, K. D. (1993). Experimental analysis of microhabitat selection by juvenile steelhead (*Oncorhynchus mykiss*) and Coho Salmon (*O. kisutch*) in a British Columbia stream. *Can. J. Fish. Sci.* **50**, 1198-1207.
- Gerstner, C. L. (1998). Use of substratum ripples for flow refuging by Atlantic cod, *Gadus morhua*. *Environ. Biol. Fishes* **51**, 455-460.
- Glauert, H. (1927). Theoretical relationships for an aerofoil with hinged flap. *Aero Res. Cttee. R and M* **1095**.
- Hayes, W. D. (1953). Wave riding of dolphins. *Nature* **172**, 1060.
- Heggenes, J. (1988). Effects of short-term flow fluctuations on displacement of, and habitat use by, brown trout in a small stream. *Trans. Am. Fish. Soc.* **117**, 336-344.
- Heggenes, J. (2002). Flexible summer habitat selection by wild, allopatric brown trout in lotic environments. *Trans. Am. Fish. Soc.* **131**, 287-298.
- Igarashi, T. (1999). Flow resistance and Strouhal number of a vortex shedder in a circular pipe. *Jpn. Soc. Mech. Eng.* **42**, 586-595.
- Issa, R. I. (1985). Solution of the implicitly discretised fluid flow equations by operator splitting. *J. Comp. Phys.* **62**, 40-65.
- Lauder, B. E. and Sharma, B. I. (1974). Application of the energy dissipation model of turbulence to the calculation of flow near a spinning disc. *Lette. Heat Mass Trans.* **1**, 131-138.
- Liao, J. C. (2004). Neuromuscular control of trout swimming in a vortex street: Implications for energy economy during the Kármán gait. *J. Exp. Biol.* **207**, 3495-3506.
- Liao, J. C. (2006). The role of the lateral line and vision on body kinematics and hydrodynamic preference of rainbow trout in turbulent flow. *J. Exp. Biol.* **209**, 4077-4090.
- Liao, J. C. (2007). A review of fish swimming mechanics and behaviour in altered flows. *Philos. Trans. R. Soc. Lond. B. Biol. Sci.* **362**, 1973-1993.
- Liao, J. C., Beal, D. N., Lauder, G. V. and Triantafyllou, M. S. (2003a). The Karman gait: novel body kinematics of rainbow trout swimming in a vortex street. *J. Exp. Biol.* **206**, 1059-1073.
- Liao, J. C., Beal, D. N., Lauder, G. V. and Triantafyllou, M. S. (2003b). Fish exploiting vortices decrease muscle activity. *Science* **302**, 1566-1569.
- McLaughlin, R. L. and Noakes, D. L. G. (1998). Going against the flow: an examination of the propulsive movements made by young brook trout in streams. *Can. J. Fish. Aquat. Sci.* **55**, 853-860.
- Montgomery, J. C., McDonald, F., Baker, C. F., Carton, A. G. and Ling, N. (2003). Sensory integration in the hydrodynamic world of rainbow trout. *Proc. R. Soc. Lond. B. Biol. Sci.* **270**, 195-197.
- OpenCFD Ltd (2009). OpenFOAM User Guide 1.5. www.openfoam.org.
- Patankar, S. (1980). *Numerical Computation of Internal and External Flows*. London, UK: Taylor and Francis.
- Pavlov, D. S., Lupandin, A. I. and Skorobogatov, M. A. (2000). The effects of flow turbulence on the behaviour and distribution of fish. *J. Ichthyol.* **40**, 232-261.
- Shih, T. H., Liou, W. W., Shabbir, A., Yang, Z. and Zhu, J. (1995). A new $k-\epsilon$ eddy-viscosity model for high Reynolds number turbulent flows-model development and validation. *Computers Fluid* **24**, 227-238.
- Shuler, S. W., Nehring, R. B. and Fausch, K. D. (1994). Diel habitat selection by brown trout in the Rio Grande river, Colorado, after placement of boulder structures. *N. Am. J. Fish. Manage.* **14**, 99-111.
- Smith, D. L. and Brannon, E. L. (2005). Response of juvenile rainbow trout to turbulence produced by prismatic shapes. *Trans. Am. Fish. Soc.* **134**, 741-753.
- Sutterlin, A. M. and Waddy, S. (1975). Possible role of the posterior lateral line in obstacle entrainment by brook trout (*Salvelinus fontinalis*). *J. Fish. Res. Bd. Can.* **32**, 2441-2446.
- Swanson, C., Young, P. S. and Cech, J. J. (1998). Swimming performance of delta smelt: maximum performance and behavioural and kinematic limitations of swimming at submaximal velocities. *J. Exp. Biol.* **201**, 333-345.
- Versteeg, H. K. and Malalasekera, W. (1995). *An Introduction to Computational Fluid Dynamics* 1. Harlow: Longman.
- Vogel, S. (1996). *Life in Moving Fluids*. Princeton University Press.
- Webb, P. W. (1998). Entrainment by river chub *Nocomis micropogon* and smallmouth bass *Micropterus dolomieu* on cylinders. *J. Exp. Biol.* **201**, 2403-2412.